K_L = overall mass transfer coefficient for initial dissolution
K_L^* = overall mass transfer coefficient for exchange in saturated solution
K_i = equilibrium constant of step i
K_m = combined rate constant Table 1)
$[M]$, $[M_i]$, $[M_s]$ = concentration of mixed micelles in the bulk solution, at the interface, and on the surface, respectively, moles/cm^3
n = constant, equal to $(d[F]/dt)/(d[M]/dt)$
R = radius of rotating disk
Re = Reynolds number
$[S]$ = free sites for micelle adsorption
$[S_o]$ = total sites
t = time
v_{max} = combined rate constant (Table 1)
ξ = constant, equal to $[F(\text{sat})]/[B]$
ν = kinematic viscosity
ω = angular velocity of rotating disk

LITERATURE CITED

Albright, J. G., and R. Mills, "Diffusion in the Ternary System Labeled Urea-Urea-Water," *J. Phys. Chem.*, **69**, 3120 (1965).

Aris, R., *The Mathematical Theory of Diffusion and Reaction Permeable Catalysts*, Clarendon Press, Oxford, England (1975).

Chan, A. F., "The Kinetics of Detergency," Ph.D. thesis, Carnegie-Mellon Univ., Pittsburgh, Pa. (1976).

———., E. L. Cussler, and D. F. Evans, "Mechanism of Solubilization in Detergent Solution" (1976).

Curran, P. F., A. E. Taylor, and A. K. Solomon, "Tracer Diffusion and Unidirectional Fluxes," *Biophys. J.*, **7**, 879 (1967).

Cussler, E. L., *Multicomponent Diffusion*, Elsevier, New York (1976).

Dunlop, P. J., "Relations Between Mutual and Tracer Diffusion Coefficients," *J. Phys. Chem.*, **69**, 1693 (1965).

Eisenberg, M., C. W. Tobias, and C. R. Wilke, "Mass Transfer at Rotating Cylinders," *Chem. Eng. Progr. Symposium Ser. No. 16*, **51**, 1 (1955).

Elworthy, P. H., A. T. Florence, and C. B. McFarlane, *Solubilization by Surface-Active Agents*, Chapman and Hall, London, England (1968).

Hougen, O. A., and K. M. Watson, *Chemical Process Principles, Part III, Kinetics and Catalysis*, Wiley, New York (1943).

Jones, T. G., "Dirt Removal," in *Surface Activity and Detergency*, K. Durham, ed., MacMillan, London, England (1961).

Kratohvill, J. P., and H. T. Dellicolli, "Measurement of the Size of Micelles: The Case of Sodium Taurodeoxycholate," *Fed. Proc. Fed. Amer. Soc. Exp. Biol.*, **29**, 1335 (1970).

Laidler, K. J., *Chemical Kinetics*, 2 ed., McGraw Hill, New York (1965).

Lawrence, A. S. C., "Polar Interaction in Detergency," in *Surface Activity and Detergency*, K. Durham, ed., MacMillan, London, England (1961).

Levich, V. G., *Physiochemical Hydrodynamics*, Chapt. II, Prentice-Hall, Englewood Cliffs, N. J. (1962).

Schott, H., "Removal of Organic Soil from Fibrous Substrates" and "Removal of Particulate Soil," in *Detergency: Theory and Test Methods*, W. G. Cutler and R. C. Davis, ed., Marcel Dekker, New York (1972).

Schwartz, A. M., "Recent Advances in Detergency Theory," *J. Am. Oil Chemist Soc.*, **48**, 566 (1971).

Sehlin, A. C., E. L. Cussler, and D. F. Evans, "Diffusion in Bile and its Implications on Detergency," *Biochim. Biophys. Acta*, **388**, 385 (1975).

Small, D. M., S. A. Penkett, and C. Chapman, "Studies on Simple and Mixed Bile Salt Micelles by NMR Spectroscopy," *ibid.*, **176**, 178 (1969).

Stewart, W. E., and R. Prober, "Matrix Calculation of Multicomponent Mass Transfer in Isothermal Systems," *Ind. Eng. Chem. Fundamentals*, **3**, 224 (1964).

Tao, J. C., E. L. Cussler, and D. F. Evans, "Accelerating Gallstone Dissolution," *Proc. Natl. Acad. Sci.*, **71**, 3917 (1974).

Toor, H. L., "Solution of the Linearized Equations of Multicomponent Mass Transfer," *AIChE J.*, **10**, 448, 460 (1964).

Manuscript received June 11, 1976; revision received July 12 and accepted July 16, 1976.

An Analysis of Slow Reactions in a Porous Particle

A one-parameter volume reaction model is developed by a simplified analytical approach to describe reaction of a gas and a consumable solid in a porous particle. In this model, a modified Thiele modulus M is introduced to take into account the effect of solid reactant depletion during the reaction.

Experimental results of an isothermal carbon-carbon dioxide reaction in the temperature range from 1 130° to 1 365°K under atmospheric pressure were analyzed by the working diagrams derived from this model. A satisfactory agreement between the experimental results and those predicted by the model indicated the applicability of this model.

C. Y. WEN

and

NANCY TSAI WU

Department of Chemical Engineering
West Virginia University
Morgantown, West Virginia 26506

SCOPE

A number of models dealing with the reaction between a gas and a consumable solid in a porous particle have been reported. Some examples are the unreacted-core shrinking model, the homogeneous model, the zone-reaction model, and the structural model. However, the applicability of the models is often limited, either owing to simplifications or to assumptions made in deriving the models. This is especially true in reference to the solid structure. Hence, the objective of this study is to develop a simple volume reaction model that can be used to simulate the overall performance of the heterogeneous reaction. Experiments were performed to verify the validity of this model.

CONCLUSIONS AND SIGNIFICANCE

An isothermal carbon-carbon dioxide reaction system was selected to verify the volume reaction model. The kinetic reaction rate was found to be first order with respect to both carbon and carbon dioxide. The activation energy obtained by fitting the curve with the least-square method to the experimental data was 69 Kcal/mole (Figure 6). This value falls within the range of the activation energies reported in the literature (Table 1).

The working diagrams derived from the volume reaction model were employed to analyze the kinetic data and to interpret the overall performance of carbon-carbon dioxide reaction from a macroscopic view point. The initial Thiele modulus ϕ_{vo}, evaluated through the working diagram of this model, agrees with that calculated from the experimental data.

The initial Thiele modulus ϕ_{vo} characterizes the reaction system in this model. Once the initial Thiele modulus is determined, the entire reaction path can be easily interpreted through this model.

The volume reaction model provides a simplified and a satisfactory interpretation of the experimental results. The model takes into account the intraparticle diffusion for the reactions which are not exceedingly rapid and on the particles whose porous structure remains essentially unchanged. The model also incorporates the concentration dependence of the solid reaction which is a factor neglected by most investigators.

The model provides a satisfactory simulation for the carbon-carbon dioxide reaction. Whether this model may be applied to other systems remains to be investigated.

A number of gas-solid reaction models have been proposed which may be classified according to two distinct features. Models in which the reaction is considered to occur only at the reaction interface are called surface-reaction models. The surface-reaction model is also known as the unreacted-core-shrinking model, the shell-progressing model, or simply the unreacted-core-model. Those models in which the reaction occurs uniformly throughout the interior of the solid phase are known as volume-reaction models.

A number of models representing intermediate conditions have also been proposed. These models are merely extensions of the surface-reaction model and volume-reaction model, with emphasis being placed on solid structural effects on the reaction mechanism. Recently, several investigators (Hashimoto and Silveston, 1973, 1973*a*; Ishida and Shirai, 1969, 1969*a*; Ishida and Wen, 1971, 1971*a*; Park and Levenspiel, 1975; Petersen, 1957; Petersen and Wright, 1955; Sohn and Szekely, 1972, 1973; Szekely and Evans, 1970, 1971, 1972, 1972*a*; Szekely et al., 1973; Tien and Turkdogan, 1970, 1972; Turkdogan et al., 1968, 1969, 1970, 1970*a*, 1972; Walker et al., 1953, 1959; Wang and Wen, 1972; Wen, 1968; Wen and Wang, 1970) have focused their attention on the structure of the solid reactant and have found that the solid structure plays an important role in the heterogeneous reaction.

TABLE 1. SUMMARY OF ACTIVATION ENERGIES OF CARBON-CARBON DIOXIDE REACTION

Investigator	(yr)	Reaction condition (°C)	Activation energy (Kcal/g-mole)	Type and shape of carbon
Drakeley	(1931)	950-1 100	50, 70	Several types of cokes (packed beds)
Mayers	(1934)	950-1 300	39	Spectroscopic coke (packed beds)
Mayers	(1939)	850-1 150	52	Acheson graphite (packed beds)
Graham	(1947)		61.5	
Long and Sykes	(1950)	700-900	59, 68	Coconut shell, charcoal (packed beds)
Walker et al.	(1953)	900-1 100	47	Gas baked carbon
		900-1 200	48	Artificial graphite
		1 200-1 400	26	Artificial graphite (5.1 cm long × 1.3 cm diameter rods)
Walker et al.	(1955)	900-1 000	43	Carbon C
			68	Graphite carbon A (5.1 cm long × 1.3 cm diameter rods)
Wicke	(1955)	850-1 000	43 ± 1.5 (with diffusion) 84 ± 3 (without diffusion)	Activated charcoal (packed beds, rods)
Rossberg and Wicke	(1956)	<950	93	Spectroscopic carbon
Ergun	(1956)	1 000-1 400	59	Ceylon graphite
		950-1 150		Activated carbon
		700-1 050		Activated graphite (1.8 mm-0.081 mm in diam. granules in fluidizing bed)
Walker and Raats	(1956)	970-1 130	66	Graphitized carbons (rods)
		1.0 atm-0.75 atm		
		>1 130, (1 392°C)	44	Graphitized carbons (rods)
Armington	(1961)	900	84	Graphite (packed beds)
Blackwood	(1962)	650-870	60-65	Electrode graphite (1.5 ± 0.5 mm in diam. granule)
Austin and Walker	(1963)	800-1 300	54	Electrode carbon (plate)
Gulbransen et al.	(1965)	1 000-1 300	88	Electrode graphite (1 cm diam. × 0.5 cm long cylinders)
		0.025 atm CO_2		
Yoshida and Kunii	(1969)	900-1 200	54	Graphite (1.5 cm diam. sphere)
Turkdogan et al.	(1968)	900-1 100	73	Graphite (small particles)

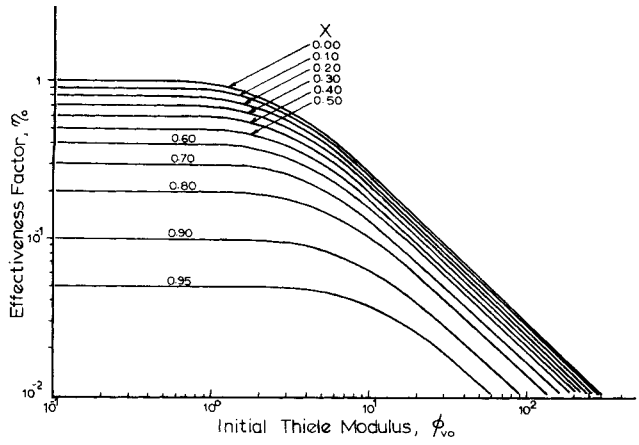

Fig. 1. The effectiveness factor for the volume reaction model showing the change of the reaction rate as the solid reactant depletes.

In this study, the derivation of the proposed model was based on the volume-reaction model with the consideration of solid reactant depletion from a macroscopic point of view, that is, a first-order dependence on the solid and gaseous reactants.

The reaction system selected to test the model was the carbon-carbon dioxide reaction system. Table 1 summarizes the previous studies on the carbon-carbon dioxide reaction system indicating various types and shapes of carbon and reaction conditions by different investigators. The activation energies reported by these previous studies are also listed in Table 1.

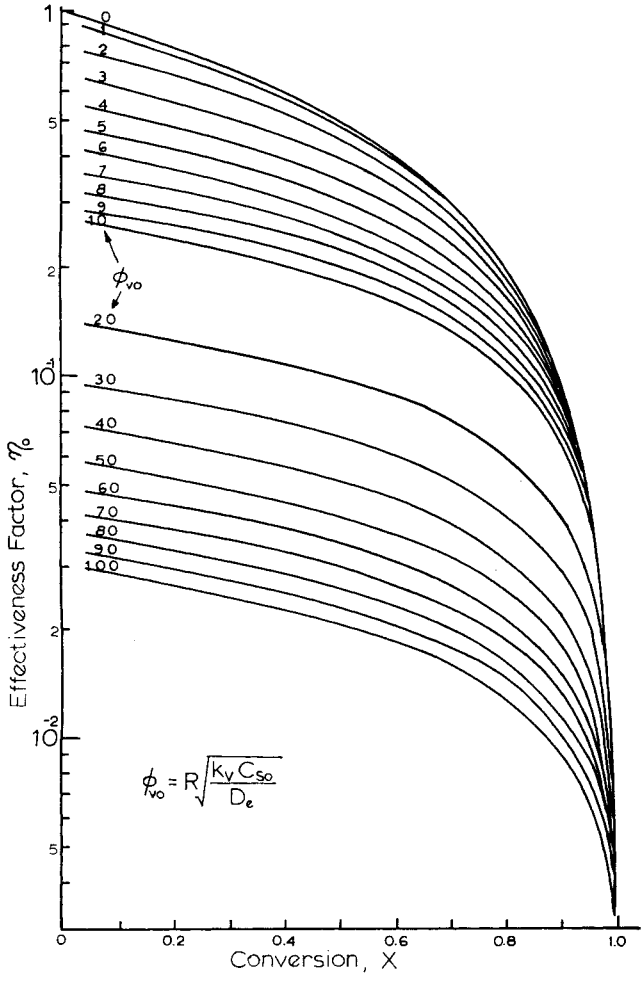

Fig. 2. The effectiveness factor for the volume reaction model in terms of initial Thiele modulus showing the effect of solid reactant depletion.

MATHEMATICAL MODEL

The model developed is based on the following assumptions and experimental conditions:

1. The pseudo steady state of gaseous components within the solid particle is applicable.
2. The effective diffusivity is considered a constant.
3. The reaction occurs under such conditions that gas film resistance is negligible.
4. The reaction is first order with respect to the gas and solid reactants.
5. The bulk flow within the particle due to diffusion is negligible.
6. An isothermal condition is maintained.
7. The useful surface area for the carbon-carbon dioxide reaction within the solid particle remains unchanged during the reaction.

For a slow reaction, the solid concentration profile and variation within the solid phase are expected to change slowly and uniformly when the above conditions prevail in the system. Although the local rate of reaction within the solid depends on the local solid concentration, for an approximation of the reaction rate an average bulk solid concentration can be used to approximate the local solid concentration. The average bulk solid concentration which can be represented by the overall solid conversion X is expressed in the following equations:

$$\overline{C}_S^* = \frac{\int_o^R C_S^* \, (4\pi r^2) \, dr}{\frac{4}{3}\pi R^3} = 3\int_o^1 C_S^* \, \xi^2 \, d\xi \qquad (1)$$

and

$$\overline{C}_S^* = 1 - X \qquad (2)$$

Thus, a material balance can be derived for a spherical particle as follows:

$$\frac{d^2 C_A^*}{d\xi^2} + \frac{2}{\xi}\frac{dC_A^*}{d\xi} = \phi_{vo}^2 (1 - X)\, C_A^* \qquad (3)$$

Here, a modified Thiele modulus M is introduced to take into account the effect of solid reactant depletion. M is defined as

$$M \equiv \phi_{vo}(1 - X)^{1/2} \qquad (4)$$

where ϕ_{vo} is the initial Thiele modulus and is characteristic of the reaction system, representing chemical reaction effect over diffusional effect. This parameter characterizes the uniqueness of the volume reaction model, since the effect of solid reactant depletion during the reaction can be incorporated into the modulus M. Thus, Equation (3) becomes

$$\frac{d^2 C_A^*}{d\xi^2} + \frac{2}{\xi}\frac{dC_A^*}{d\xi} = M^2 C_A^* \qquad (5)$$

with the boundary conditions given as follows:

$$C_A^* = 1, \quad \text{at} \quad \xi = 1 \qquad (6)$$

$$\frac{dC_A^*}{d\xi} = 0, \quad \text{at} \quad \xi = 0 \qquad (7)$$

Thus, the reaction system can be described by an ordinary differential equation [Equation (5)] containing a solid concentration term which implicitly relates to the overall solid conversion X.

The solution of Equation (5) is

$$C_A^* = \frac{\sinh M\,\xi}{\xi \sinh M} \qquad (8)$$

The effectiveness factor η_o for an overall solid conversion or for any instant during the reaction is defined and can be derived as follows:

$$\eta_o = \frac{\text{actual rate of reaction}}{\text{reaction rate based on the bulk concentration of gas and the initial solid concentration}} \tag{9}$$

$$= \frac{(4\pi R^2)\left(-D_e \frac{dC_A}{dr}\Big|_R\right)}{\left(\frac{4}{3}\pi R^3\right)(k_v C_{So} C_{Ao})}$$

$$= (1-X)\left(\frac{3}{M}\right)\left(\frac{1}{\tanh M} - \frac{1}{M}\right) \tag{10}$$

A plot of η_o vs. ϕ_{vo} for the various levels of conversion can be constructed based on Equation (10). The result is shown in Figure 1. If ϕ_{vo} is considered a parameter, a plot of η_o vs. X can be made as shown in Figure 2. Either Figures 1 or 2 can serve as a working diagram to analyze the heterogeneous reaction system. These working diagrams have been applied in analyzing the experimental results obtained in this study. It should be noted that η_o in Figure 2 is directly proportional to the conversion rate dX/dt.

EXPERIMENTAL

Equipment

A schematic diagram of the thermobalance is shown in Figure 3. The heated section of the reactor is 109 cm long and is made of 3.8 cm schedule 40, type 310 stainless steel pipe. The reactor column is heated by three sections of thermoshell electric heating elements. Each section is 30.5 cm long and 4.8 cm in diameter and is rated at 1 200 W/section. The bottom section is controlled by a proportional controller. The other two sections are controlled by an on-off set point controller. The bottom section of the reactor column is packed with 1.3 cm Intalox saddle packings to a height of 38 cm for better flow and temperature distribution of the gas. Seven thermocouples are installed along the reactor column at different positions to control and measure the reactor temperatures. Thermocouple temperatures are recorded by a Honeywell twelve-point Electronik Recorder at a rate of 5 cycles/min, or 1 point/s. The weight of the sample is recorded by a force transducer on a Mosely model 680 recorder. The gas flow rate is controlled by a flowmeter prior to the inlet of the reactor.

The schematic diagram of the equipment set up is shown in Figure 4.

Preparation of Solid Particles

Activated charcoal of USP grade manufactured by Merck and Company, Inc., was used as the solid reactant. Kaiser Refractories specially prepared fire clay was used as an inert material in the solid particles. The absolute density measured by a pycnometer was 1.637 g/cm^3 for activated charcoal and 2.040 g/cm^3 for fire clay.

The solid spheres used in the experiment were prepared by mixing a desired proportion of activated charcoal with fire clay. The proper amount of water was added to the powder mixture to form a well-mixed homogeneous thick paste which was then molded into balls of desired size. The balls were allowed to dry at room temperature for about 2 wk. When dry, the balls were stored in a 316 stainless steel box which served as an enclosure for a nitrogen blanket. Nitrogen gas was purged into the box to expel the air; then the box was heated in the oven to 815°C for at least 30 min as nitrogen gas passed continuously through the box. This treatment removed the moisture and other decomposable compounds from the solid balls. The fire clay is an impure form of Kaolin and gives off water molecules at about 600°C according to the reaction

$$Al_2Si_2O_5(OH)_4 \rightarrow Al_2O_3 \cdot 2SiO_2 + H_2O_{(g)}\uparrow$$

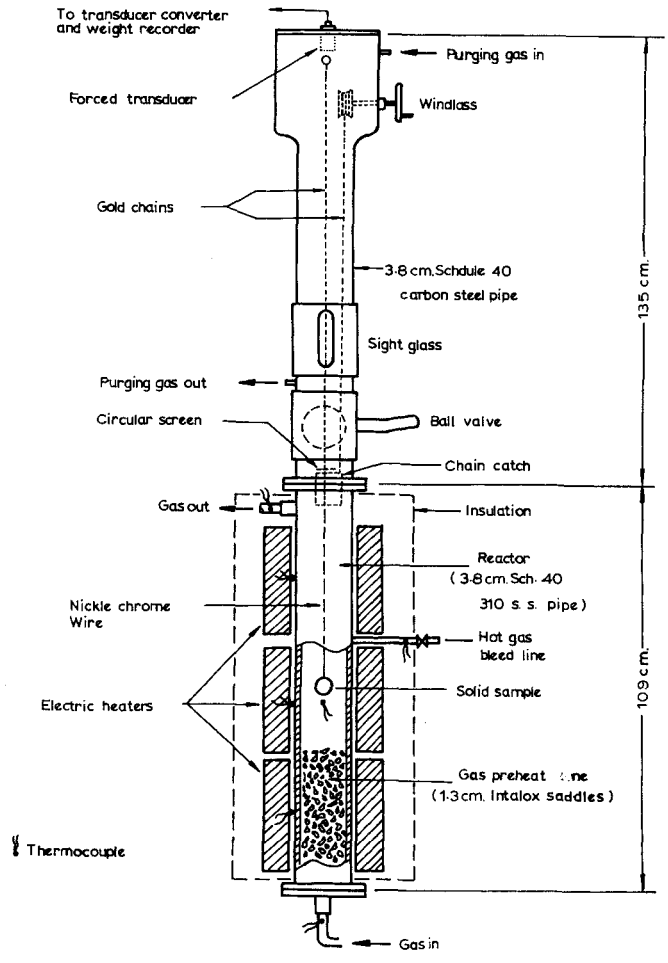

Fig. 3. Thermobalance proper used in experimentation.

The introduction of nitrogen during the heat treatment prevents a side reaction of carbon with air in the oven. After the particles had cooled, they were quickly sealed in a bottle containing desiccant.

Three concentrations of activated charcoal, 23.4, 30.0, and 40.0%, were used to prepare the solid particle. The heated solid particles were further analyzed and their compositions confirmed by measurement of the weight loss of prepared carbon balls which were completely burned at 900°C in a carbon dioxide gas stream.

Experimental Procedure

The temperatures of the reactor were set at the desired points by two temperature controllers (on-off and proportional). A small amount of air was then continuously introduced through the reactor during the heating period to prevent the reactor from overheating. One of the seven thermocouples was located at a point approximately 0.6 cm below the solid particle. This

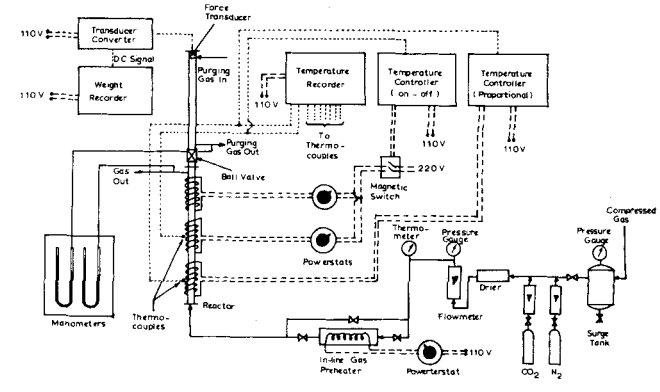

Fig. 4. Schematic diagram of equipment setup, including the wiring for electrical components.

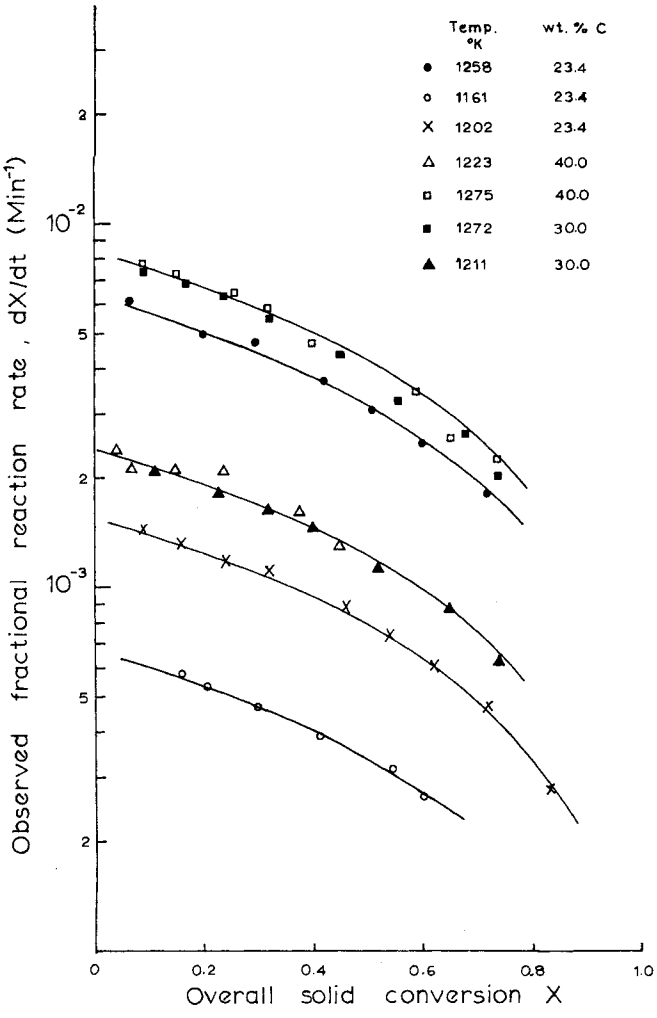

Fig. 5. Overall fractional reaction rate varies with conversion at low temperatures.

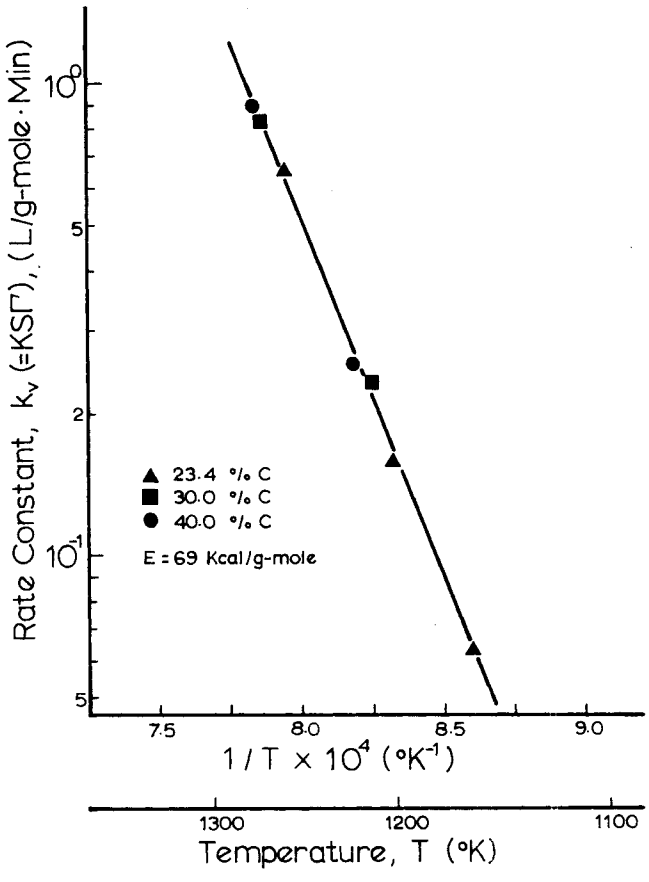

Fig. 6. Arrhenius plot of reaction rate constant k_v (=KSΓ) verifying the rate expression for the C-CO_2 reaction, which is $-dC_s/dt = k_v C_s C_{CO_2}$.

thermocouple measured the apparent temperature at the reactor center.

With the ball valve closed, the desired flow rate of air was established. The solid sample hung from a piece of nickel-chrome wire attached to a gold chain located in the center line of the reactor column. A windlass and an additional gold chain equipped with a chain catch were used to raise and lower the sample particle into the reactor chamber.

When the steady state condition was reached, nitrogen gas was used to flush the reactor for at least 20 min to expel the air in the reactor. The ball valve was then opened, and the sample was carefully lowered into the heated zone by unwinding the windlass. After the sample reached the desired position, the gas line was shifted from nitrogen to pure carbon dioxide gas or a gaseous mixture of carbon dioxide and nitrogen.

The reactor gas samples were simultaneously analyzed by a gas chromatograph which recorded the composition of reactor effluent gas either continuously or at 5 min intervals.

To terminate the experiment, the particle was raised to the upper cold section of the column and the ball valve closed. Nitrogen gas was used again to quench the reaction and cool the particle before removal from the reactor.

The solid particle was weighed before and after each run and was stored in a tightly sealed bottle for subsequent measurement of surface area and effective diffusivity.

Because of the difficulties posed by simultaneously measuring both particle temperature and weight change, these measurements were carried out separately in duplicate runs. During the reaction, particle temperature was measured by a thermocouple positioned in the center of the particles. An additional thermocouple was also inserted near the surface of the particle during its construction to secure further measurements on the particle's temperature.

Measurement of Porosity, Surface Area, and Effective Diffusivity

Porosity

The porosity of the solid particle was calculated from the absolute densities of the activated charcoal, while that of fire clay was measured by a pycnometer.

The water wetted method was also applied to determine the porosity of the solid particle. In this method the weighted solid particle was placed into a beaker of continuously boiling water. After the bubbles had ceased to form on the surface of the solid particle, the water was cooled to room temperature and the particle removed. The surface of the solid particle was first dried with a paper tissue and then weighed. Any increase in particle weight is attributed to the water which now occupies the pore space, and the porosity can then be calculated from the weight difference.

Surface Area

The commercial NUMEC surface area and density apparatus model AFA 4 was used to measure the surface area, using the Brunauer-Emmett-Teller method.

Effective Diffusivity

A diffusivity apparatus, similar to that used by SOCONY MOBIL OIL COMPANY (Mobil Method 366-59), was set up to measure the effective diffusivity of the gas within the solid sample. The binary gas system nitrogen-helium was selected for the measurement at room temperature and constant atmospheric pressure. For the molecular or Knudsen diffusion, the diffusion coefficient is inversely proportional to the square root of the molecular weight of the diffusing gaseous component. Hence, the result obtained in the nitrogen-helium system was converted into a carbon-carbon dioxide system (which is the real reaction system in this study) by multiplying by a molecular weight correction factor. This correction factor was proposed by Walker et al. (1959) in their diffusion coefficient measurement. The above correction factor can be written as

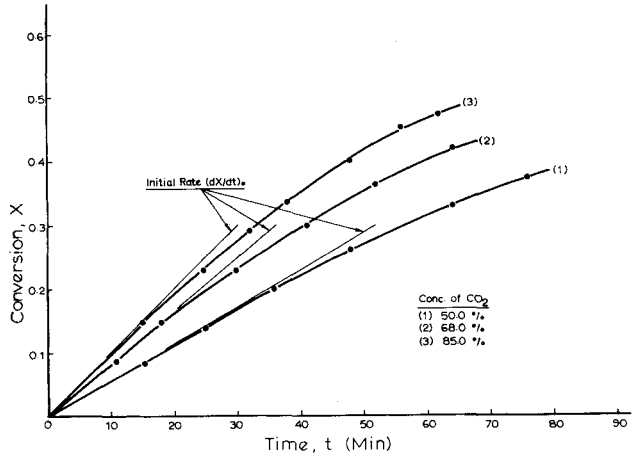

Fig. 7. The initial phase of carbon-CO_2 reaction for different compositions of CO_2-N_2 mixture at 1.01 Atm, 1360°K.

$$\sqrt{\left(\frac{1}{M_{CO_2}}+\frac{1}{M_{CO}}\right)\Big/\left(\frac{1}{M_{He}}+\frac{1}{M_{N_2}}\right)}$$

or for the present case, 0.4523.

REACTION KINETICS AND EFFECTIVE DIFFUSIVITY

The rates of carbon-carbon dioxide reaction were examined in order to obtain the rate constant k_v needed to calculate the initial Thiele modulus ϕ_{vo} from the experimental data.

The rate expression which is subsequently shown to be accurate for the present experimental domain has a form

$$-\frac{dC_S}{dt} = KS\Gamma\, C_S\, C_{CO_2} \qquad (11)$$

where the external shape and total volume of the solid particle is assumed to remain unchanged. S and Γ are the specific surface area for each type of carbon and the number of active sites per unit surface area, respectively. If S and Γ are kept constant during the reaction, then $KS\Gamma$ is a function of temperature only and can be combined to form a single reaction rate constant k_v. Since only the overall reaction rate can be measured by experimentation, the rate of weight loss during the reaction is expressed in terms of an effectiveness factor η_o as follows:

$$-\frac{dw}{dt} = \eta_o\, KS\Gamma\, w_o\, C_{Ao} \qquad (12)$$

As is evident from Equation (10) when the reaction temperature is low, the chemical reaction rate dominates the overall rate, and η_o approaches $(1 - X)$. Thus, under this condition, Equation (12) can be reduced to

$$\frac{dX}{dt} = (1 - X)\, KS\Gamma\, C_{Ao} \qquad (13)$$

Several experimental runs were carried out at low temperatures. The observed fraction rates (dX/dt) are plotted against the overall solid conversion X for each run in Figure 5. Values of $KS\Gamma$ for each run were calculated from Equation (13) and are listed in Table 4. They are also plotted against $1/T$ as shown in Figure 6. The straight line shown in the figure gives an estimated activation energy of 69 Kcal/g-mole obtained by a least-square fit. The constancy of the $KS\Gamma$ value with variation in conversion implies that the reaction is first order on the solid reactant. Three solid concentrations have been employed for the low temperature runs. For convenience, $KS\Gamma$ is replaced by k_v in the following discussion.

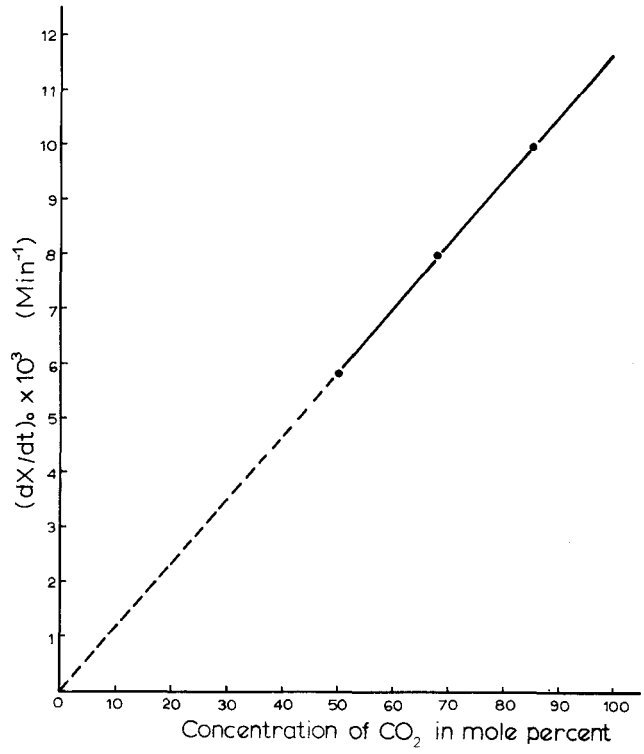

Fig. 8. Initial reaction rate is seen to be proportional to CO_2 concentration indicating C-CO_2 reaction is a first order reaction with respect to CO_2.

In general, a decrease in calculated k_v values was observed near the end of the reaction. This probably results from the change in surface area of the solid phase, especially during the final stage of the reaction. This phenomenon has also been reported by Petersen et al. (1955*a*), Walker et al. (1959), and Turkdogan et al. (1970*a*).

Three concentrations of carbon dioxide-nitrogen mixtures were used to identify the effect of carbon dioxide concentration at 1 360°K. During the early stage of reaction, η_o can be treated as a constant because it changes only slightly. Thus, Equation (12) can be integrated for the initial stage to give

$$X = \eta_o\, k_v\, C_{Ao}\, t \qquad (14)$$

Plotting conversion X vs. time t for each run, one can estimate the slope at the initial stage as shown in Figure 7. The slopes are seen to be proportional to the bulk concentration of carbon dioxide. A plot of the slope vs. molar percentage of carbon dioxide in the gaseous mixture is shown in Figure 8. A straight line through the origin indicates that the reaction is first order with respect to carbon dioxide concentration. A first-order dependency on carbon dioxide concentration in carbon-carbon dioxide reaction has also been mentioned by Ramachandra Rao and Petersen (1958) and Turkdogan et al. (1968, 1969). It can be concluded from the above discussion that the rate expression for carbon-carbon dioxide reaction represented by Equation (11) is satisfactory and accurate within the range of experimental conditions investigated.

At high temperatures, the effect of diffusion becomes significant, and therefore an accurate value of effective diffusivity D_{eA} is needed to analyze the overall reaction rate. As previously discussed, the effective diffusivity was directly measured, and the corrected values of D_{eA}/D_{fA} are presented in Table 2. The values of D_{eA}/D_{fA} for different carbon contents (and for different initial porosities) are found to vary only slightly. The average value of diffusivity ratio for the spheres with three different carbon con-

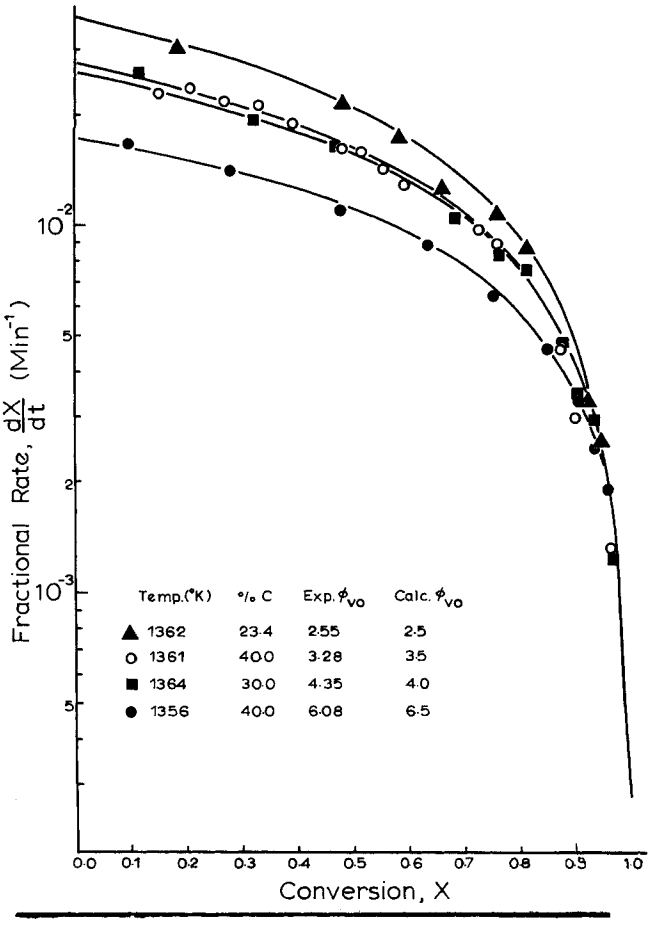

Fig. 9. Application of the working diagram (Fig. 2) showing how data are fitted to obtain the initial Thiele modulus, ϕ_{vo}, at 1 atm. and 100% CO_2.

TABLE 2. MEASURED EFFECTIVE DIFFUSIVITY (D_{eA}/D_{fA}) WITH D_{fA} = 0.149 cm^2/s AT 27°C FOR CARBON-CARBON DIOXIDE SYSTEM

23.4% activated charcoal

Average porosity	0.510	0.556	0.591	0.653	0.663
D_{eA}/D_{fA}	0.039	0.041	0.044	0.049	0.053

Average D_{eA}/D_{fA} = 0.045

30.0% activated charcoal

Average porosity	0.553	0.576	0.631	0.683	0.727
D_{eA}/D_{fA}	0.035	0.041	0.044	0.047	0.051

Average D_{eA}/D_{fA} = 0.044

40.0% activated charcoal

Average porosity	0.590	0.641	0.696	0.754	0.793
D_{eA}/D_{fA}	0.040	0.042	0.049	0.051	0.053

Average D_{eA}/D_{fA} = 0.047

Overall average D_{eA}/D_{fA} = 0.045

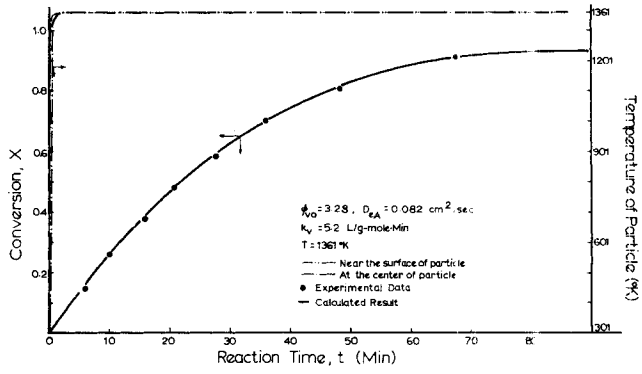

Fig. 10. Experimental and calculated time-conversion curve indicating close agreement.

tents (23.4, 30.0, and 40.0%) and with the corresponding porosities is 0.045 as listed in Table 2.

In order to assess the significance of the intraparticle diffusion, the surface area and porosity of the sample were directly measured. The result of the two methods of porosity measurement (described previously) indicates that the values are essentially the same.

The mean pore radii were calculated from the pore volume and surface area by assuming that the pores are uniform and cylindrical. The values of mean pore radii, porosity, and surface area are listed in Table 3. The mean pore radius is less than 100Å, while the mean free path of carbon-carbon dioxide pair at 1 000°C and 1 atm is about 3 000Å. Hence, the measured effective diffusivity appears too large for the Knudsen diffusion. This inconsistency is apparently due to the complicated solid structure of the sample in which micropores and macropores coexist. In addition, from the work of Turkdogan et al. (1970), the pore shape of the various types of carbons cannot be assumed as a uniform cylinder but has an irregular shape. Moreover, the calculated value of mean pore radius is an overall average pore size and does not indicate the pore size distribution within the solid particle. Nevertheless, it appears that the major part of the diffusion process takes place in macropores (Satterfield et al., 1963, 1970).

DISCUSSION AND COMPARISON OF RESULTS

In Figure 9, observed fractional reaction rates (dX/dt) were plotted vs. overall solid conversion X. By superimposing the experimental data on Figure 2, the value of ϕ_{vo} can be estimated from the curve which fitted the data.

TABLE 3. MEASURED SURFACE AREA, CALCULATED POROSITY, AND CALCULATED MEAN PORE RADIUS OF SOLID PARTICLE

	23.4%C				30%C	40%C
Porosity, ϵ	0.510	0.556	0.591	0.635	0.553	0.590
Specific surface area, S (m^2/g)	395	389	358	169	490	559
Bulk density of solid particle, ρ_b (g/cm^3)	1.060	0.988	0.930	0.857	0.941	0.831
Void volume of solid particle, V_g (cm^3/g)	0.481	0.563	0.635	0.741	0.588	0.710
Mean pore radius, $r = 2V_g/S$ (Å)	24.4*	28.9	35.5	87.5	24.0*	25.4*

* These properties are for the unreacted particles. The values marked '*' show that the initial mean pore sizes, and hence the internal pore structures, are the same regardless of the carbon content.

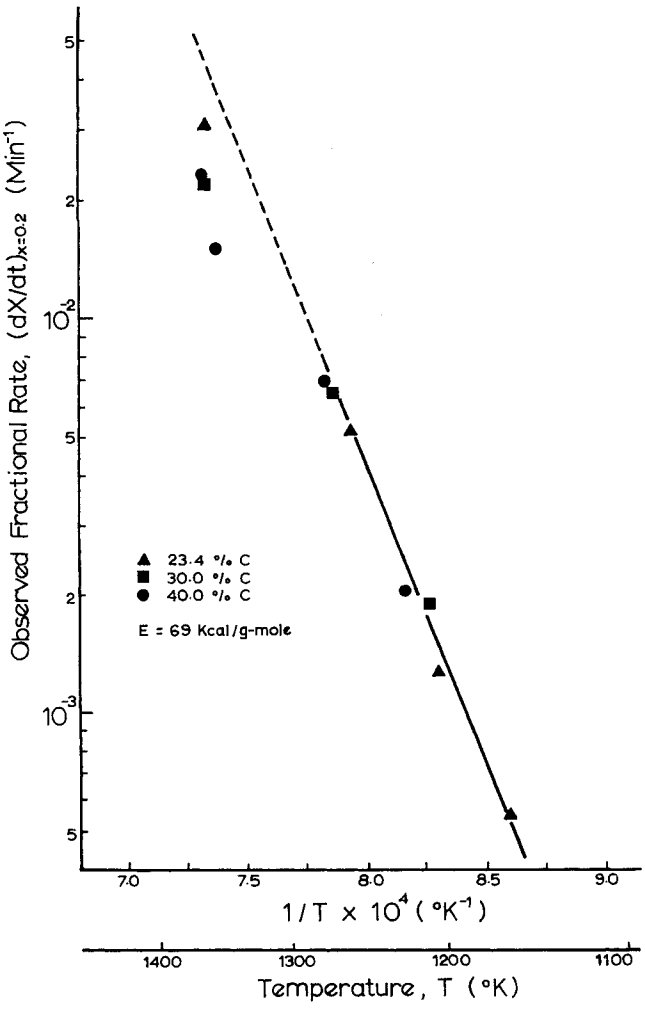

Fig. 11. Arrhenius plot of the observed reaction rate at 20% carbon conversion showing that at high temperature the intraparticle diffusion tends to affect the overall reaction rate.

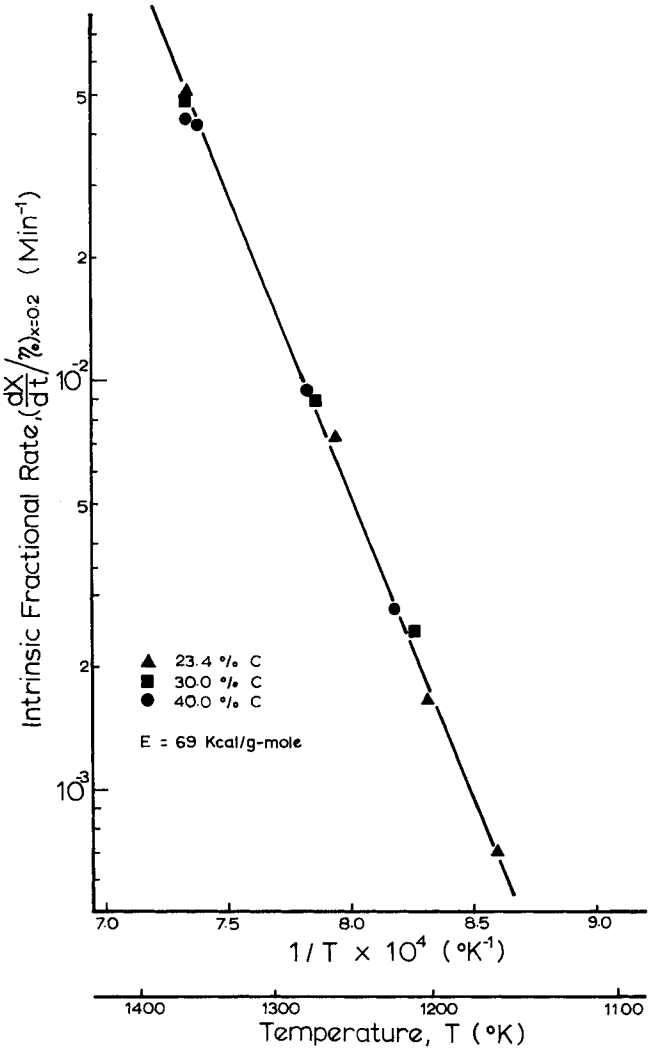

Fig. 12. Effectiveness factor is used as a correction factor to obtain the intrinsic reaction rate at 20% carbon conversion.

The value of ϕ_{vo} from the best fitted curve and the value of ϕ_{vo} calculated directly from the experimental data are shown in Table 4. The good agreement between these values of ϕ_{vo} is an indication that the proposed model is applicable in the present reaction system. The values of k_v for high temperatures can be read from Figure 6 by extrapolation and are also listed in Table 4.

TABLE 4. CALCULATED ϕ_{vo} AND CALCULATED k_v (OR $KS\Gamma$) FROM THE EXPERIMENTAL DATA AND THE ϕ_{vo} OBTAINED FROM THE BEST CURVE FIT

	Run No.	Diam. of particle, d (cm)	Initial solid conc. C_{So} (g-mole/cm^3)	$k_v = KS\Gamma$ (1/g-mole min)	Calculated ϕ_{vo}†	Curve fit ϕ_{vo}
23.4% C	1*	1.927	0.0207	0.656	1.62	1.0
	8*	1.915	0.0207	0.064	0.52	≃0.0
	9*	1.873	0.0207	0.157	0.81	1.0
	10	1.157	0.0207	5.2	2.55	2.5
40.0% C	14	1.285	0.0277	5.2	3.28	3.5
	30	2.532	0.0276	4.6	6.08	6.5
	18*	1.913	0.0276	0.251	1.18	1.0
	19*	1.229	0.0278	0.890	1.38	≃0.0
30.0% C	21*	1.271	0.0237	0.826	1.27	≃0.0
	22*	1.142	0.0234	0.235	0.62	≃0.0
	23	1.849	0.0236	5.2	4.35	4.0

* Runs at low temperature, k_v calculated from experimental data.
† $\phi_{vo} = R(k_v C_{So}/D_{eA})^{1/2}$, with $D_{eA}/D_{fA} = 0.045$.

Further evidence to substantiate the model can be found from the plots of conversion X vs. time t shown in Figure 10. The points represent the experimental data. The curve passing through the points is calculated from the following equation with $\phi_{vo} = 3.8$ and $k_v = 5.2$ (l/g-mole · min). The $X - t$ equation is derived from the definition of the effectiveness factor based on the model. It is an implicit equation having the form

$$\ln\{(\cosh\phi_{vo})(\phi_{vo} - \tanh\phi_{vo})\} - \ln\{(\cosh M)(M - \tanh M)\} = (3/2)k_v C_{Ao} \cdot t \quad (15)$$

As can be seen from Figure 10, the experimental results agree closely with that predicted by the volume reaction model. In Figure 10, the broken lines are the temperatures of the solid particle measured at center and near the surface by two small thermocouples which indicate that an isothermal condition prevailed.

If the observed fractional rate (dX/dt) is plotted vs. $1/T$ at 20% conversion from 1160° to 1365°K as shown in Figure 11, a straight line can be drawn through the points in the low-temperature region leaving the points at high-temperature region below the straight line. This is expected because the intraparticle diffusion significantly affects the overall reaction rate at high temperature. This

phenomenon has been discussed by many investigators (Wicke, 1955).

The effectiveness factor η_o can be used to interpret the extent of the intraparticle diffusion effect over the true chemical reaction rate. From Figure 1, the effectiveness factor can be estimated for each run shown in Figure 11 at 20% conversion based on the calculated value of ϕ_{vo} from Table 4. When we use the effectiveness factor, the observed fractional rate can be converted into the intrinsic chemical reaction rate. The plot of those intrinsic fractional rate vs. $1/T$ is shown in Figure 12, indicating a straight line passing through all the points. The activation energy can then be estimated to be about 69 Kcal/g-mole.

NOTATION

C_A = molar concentration of gaseous reactant within the solid particle, C_{Ao} in bulk phase (mole/L^3)
C_A^* = C_A/C_{Ao} (−)
C_S = molar concentration of solid reactant, C_{So} initial concentration (mole/L^3)
C_S^* = C_S/C_{So} (−)
D_e = effective diffusivity of gas, D_{eA} for gaseous reactant A (L$^2/\theta$)
D_f = molecular diffusivity of gas, D_{fA} for gaseous reactant A (L$^2/\theta$)
E = activation energy of reaction rate constant k_v (H/mole)
k_v = volumetric reaction rate constant [L$^{3(m+n-1)}$/mole$^{(m+n-1)}$ θ]
K = Arrhenius type of rate constant (L^{3}M/mole θ)
M = $\phi_{vo}(1-X)^{1/2}$, modified Thiele modulus (−)
m, n = order of reaction for solid reactant and gaseous reactant, respectively (−)
r = distance from the center of the sphere (L)
$\bar{r}$ = mean pore radius (L)
R = characteristic diameter of solid particle, or the radius of the solid sphere (L)
S = specific surface area of carbon (L^2/M)
t = time (θ)
T = temperature (T)
w = weight of carbon in the solid particle (M)
w_o = initial weight of carbon in the solid particle (M)
X_A = mole fraction of gaseous reactant A (−)
X = overall fractional conversion of solid reactant (−)
η_o = effectiveness factor (−)
ξ = r/R (−)
ϕ_{vo} = $R(k_v C_{so}/D_e)^{1/2}$, initial Thiele modulus (−)
Γ = number of the active sites per unit surface area of the solid reactant (#/L^2)

LITERATURE CITED

Armington, A. F., "Surface Effects on the Low Temperature Gasification of Carbons," Ph.D. thesis, Penn. State Univ. (1961).

Austin, L. G., and P. L. Walker, "Effect of Carbon Monoxide in Causing Nonuniform Gasification of Graphite by Carbon Dioxide," *AIChE J.*, **9**, 303 (1963).

Blackwood, J. D., "Reaction of Graphite with Carbon Dioxide and Hydrogen," *Austr. J. Appl. Sci.*, **13**, No. 3, 199 (1962).

Drakeley, T. J., "Reactivity of Coke," *Soc. Chem. Industry J. (Trans. and Communications)*, **50**, No. 35, 319T (1931).

Ergun, S., "Kinetics of Reaction of Carbon Dioxide with Carbon," *J. Phys. Chem.*, **60**, 480 (1956).

Graham, H. S., "Gasification of Carbon In A Fluidized Powder Bed," D.Sc. thesis, Mass. Inst. Technol., Cambridge (1947).

Gulbransen, E. A., K. F. Andrew, and F. A. Brassart, "Reaction of Hydrogen with Graphite," *Electrochem. Soc. J.*, **12**, No. 1, 49 (1965).

Hashimoto, K., and P. L. Silveston, "Gasification: Part I. Isothermal Kinetic Control Model for a Solid With a Pore Size Distribution," *AIChE J.*, **19**, 259 (1973).

———., *Ibid.*, Part II. Extension to Diffusion Control," 268 (1973a).

Ishida, M., and T. Shirai, "Graphical Representation of Solid-Gas Reactions Based on Unreacted Core Model," *Chem. Eng. J. (Japan)*, **2**, 175 (1969).

———., "Non-isothermal Analysis of Unreacted-Core Model For the Burning Rate of Single Carbon-Cement Spheres," *ibid.*, 180 (1969*a*).

Ishida, M., and C. Y. Wen, "Comparison of Zone-Reaction Model and Unreacted-Core Shrinking Model in Solid-Gas Reaction—I Isothermal Analysis," *Chem. Eng. Sci.*, **26**, 1031 (1971).

———., "Comparison of Zone-Reaction Model and Unreacted-Core Shrinking Model in Solid-Gas Reaction—II Non-isothermal Analysis," *ibid.*, 1043 (1971*a*).

Long, F. J., and K. W. Sykes, "The Catalysis of the Oxidation of Carbon," *J. Chim. Phys.*, **47**, 361 (1950).

Mayers, M. A., "The Rate of Reduction of CO_2 by Graphite," *J. Am. Chem. Soc.*, **56**, 70 (1934).

———., "The Reduction of Carbon Dioxide by Graphite and Coke," *ibid.*, **61**, 2053 (1939).

Park, J. Y., and O. Levenspiel, "The Crackling Core Model for the Reaction of Solid Particles," *Chem. Eng. Sci.*, **30**, 1207 (1975).

Petersen, E. E., "Reaction of Porous Solids," *AIChE J.*, **3**, 443 (1957).

———., and C. C. Wright, "Reaction of Artificial Graphite With Carbon Dioxide," *Ind. Eng. Chem.*, **47**, 1624 (1955).

Petersen, E. E., P. L. Walker, Jr., and C. C. Wright, "Surface Area Development Within Artificial Graphite Rods Reacted With Carbon Dioxide from 900°C to 1300°C," *ibid.*, 1629 (1955*a*).

Ramachandra Rao, P. V. N., and E. E. Petersen, "Effect of Carbon Dioxide Concentration on Gasification of Artificial Graphite," *ibid.*, **50**, 331 (1958).

Rossberg, M., and E. Wicke, "Transportvorgaenge und Oberflaechenreaktinen bei der Verbrennung graphitischen Kohlenstoffs," *Chem. Ing. Tech.*, **28**, 181 (1956).

Satterfield, C. N., *Mass Transfer in Heterogeneous Catalysis*, Mass. Inst. Technol. Press, Cambridge (1970).

Satterfield, C. N., and T. K. Sherwood, *The Role of Diffusion in Catalysis*, Addison-Wesley (1963).

Sohn, H. Y., and J. Szekely, "A Structural Model for Gas-Solid Reactions With a Moving Boundary—III. A General Dimensionless Representation of the Irreversible Reaction Between A Porous Solid and a Reactant Gas," *Chem. Eng. Sci.*, **27**, 763 (1972).

———., "A Structural Model for Gas-Solid Reactions With A Moving Boundary—IV. Langmuir-Hinshelwood Kinetics," *ibid.*, **28**, 1169 (1973).

Szekely, J., and J. W. Evans, "A Structural Model for Gas-Solid Reactions With a Moving Boundary," *ibid.*, **25**, 1091 (1970).

———., "A Structural Model for Gas-Solid Reactions With A Moving Boundary," *ibid.*, **26**, 1901 (1971).

———., "Studies in Gas-Solid Reactions: Part I. A Structural Model for the Reaction of Porous Oxides with a Reducing Gas," *Met. Trans.*, **2**, 1691 (1972).

———., "Studies in Gas-Solid Reactions: Part II. An Experimental Studies of Nickel Oxide Reduction With Hydrogen," *ibid.*, 1699 (1972*a*).

Szekely, J., C. I. Lin, and H. Y. Sohn, "A Structural Model for Gas-Solid Reactions With A Moving Boundary—V. An Experimental Study of the Reduction of Porous Nickel-Oxide With Hydrogen," *Chem. Eng. Sci.*, **28**, 1975 (1973).

Tien, R. H., and E. T. Turkdogan, "Incomplete Pore Diffusion Effect on Internal Burning of Carbon," *Carbon*, **8**, 607 (1970).

———., "Mathematical Analysis of Nonisothermal Mass Transfer Process—Application to Oxidation of Carbon With CO_2-CO Mixtures," *ibid.*, **10**, 35 (1972).

Turkdogan, E. T., V. Komp, J. V. Vinters, and T. F. Perzak, "Rate of Oxidation of Graphite in Carbon Dioxide," *ibid.*, **6**, 467 (1968).

Turkdogan, E. T., and J. V. Vinters, "Kinetics of Oxidation of Graphite and Charcoal in Carbon Dioxide," *ibid.*, **7**, 101 (1969).

———., "Effect of Carbon Monoxide on the Rate of Oxidation of Charcoal, Graphite and Coke in Carbon Dioxide," *ibid.*, **8**, 39 (1970).

Turkdogan, E. T., R. G. Olsson, and J. V. Vinters, "Pore Characteristics of Carbons," *ibid.*, 545 (1970*a*).
Turkdogan, E. T., and J. V. Vinters, "Catalytic Oxidation of Carbon," *ibid.*, 97 (1972).
Walker, P. L., Jr., R. J. Foresti, and C. C. Wright, "Surface Area Study of Carbon-Carbon Dioxide Reaction," *Ind. Chem. Eng.*, **45**, 1703 (1953).
Walker, P. L., Jr., F. Rusinko, Jr., and E. Raats, "Changes of Macropore Distributions in Carbon Rods Upon Gasification with Carbon Dioxide," *J. Phys. Chem.*, **59**, 245 (1955).
Walker, P. L., Jr., and E. Raats, "Changes in Physical Properties of Graphitized Carbon Rods Upon Gasification with Carbon Dioxide," *ibid.*, **60**, 364 (1956).
Walker, P. L., Jr., F. Rusinko, Jr., and L. G. Austin, "Gas Reactions of Carbon," in *Advance in Catalysis*, Vol. XI, p. 133, Academic Press, New York (1959).
Wang, S. C., and C. Y. Wen, "Experimental Evaluation of Nonisothermal Solid-Gas Reaction Model," *AIChE J.*, **18**, 1231 (1972).
Wen, C. Y., and S. C. Wang, "Thermal and Diffusional Effects in Non-Catalytic Solid-Gas Reactions," *Ind. Eng. Chem.*, **62**, 30 (1970).
Wen, C. Y., "Noncatalytic Heterogeneous Solid Fluid Reaction Models," *ibid.*, **60**, 34 (1968).
Wicke, E., "Contributions to the Combustion Mechanism of Carbon," in *Fifth Symposium on Combustion*, p. 245, Reinhold, New York (1955).
Yoshida, K., and D. Kunii, "Gasification of Porous Carbon by Carbon Dioxide," *Chem. Eng. J. (Japan)*, **2**, 1170 (1969).

Manuscript received December 23, 1975; revision received July 20 and accepted July 22, 1976.

The Effect of Flow Maldistribution on Conversion in a Catalytic Packed-Bed Reactor

Part I. Analysis

MANOJ CHOUDHARY
JULIAN SZEKELY
and
SOL W. WELLER

Department of Chemical Engineering
State University of New York at Buffalo
Buffalo, New York 14214

Through the statement of the vectorial form of the Ergun equation, combined with a differential component balance, a formulation was developed describing the velocity fields and reactant concentration profiles in an isothermal packed-bed reactor in which the gas flow is nonuniform. This flow maldistribution was caused by both the preferential flow near the wall, inherent in most systems, and by the deliberate arrangement of the solid packing in the bed. The numerical solution of the governing equations showed that a nonuniform flow field had a very strong effect in distorting the concentration isopleths, particularly at intermediate conversion levels.

SCOPE

The quantitative understanding of the effect of nonuniform gas flow on the performance of packed-bed reactors is a problem of considerable practical importance in chemical reaction engineering. It has been suggested that hot spot formation and temperature excursions may well be associated with or are the direct consequence of nonuniform flow. In recent years, numerous theoretical studies have been made of nonuniform flow in packed-bed reactors (Radestock and Jeschar, 1969, 1970, 1971*a*, 1971*b*; Stanek and Szekely, 1972, 1973, 1974), and more recently direct experimental proof has been provided con-

Manoj Choudhary and Julian Szekely are with the Department of Materials Science and Engineering, Massachusetts Institute of Technology, Cambridge, Massachusetts 02139.